Dalton Transactions

PAPER

View Article Online
View Journal | View Issue

Cite this: *Dalton Trans.*, 2014, **43**, 11973

Chloride-bridged, defect-dicubane {Ln_4} core clusters: syntheses, crystal structures and magnetic properties†

Daniel M. Pajerowski,*[a] Quan Li,[b] Jason Hyun,[a,d] Cindi L. Dennis,[a] Daniel Phelan,[c] Pengfei Yan,[b] Peng Chen[b] and Guangming Li*[b]

Received 5th May 2014,
Accepted 13th June 2014

DOI: 10.1039/c4dt01329h

www.rsc.org/dalton

Three chloride-bridged lanthanide compounds, $[Ln_4Cl_6(CH_3OH)_{12}(OH)_2]\cdot 4Cl\cdot 2CH_3OH$ [Ln = Gd (**1**), Dy (**2**) and Er (**3**)], have been unexpectedly isolated by the reactions of $LnCl_3\cdot 6H_2O$ and *N*,*N*′-bis(salicylidene)-1,2-(phenylene-diamine) (H_2L). X-ray crystallographic analysis reveals a triclinic cell with a unique defect-dicubane {Ln_4} core and the structure across this series is nominally isomorphic. Measurements of direct current magnetic susceptibility and isothermal magnetization give insight into the relevant cluster Hamiltonians for **1**, **2**, and **3**, and alternating current susceptibility shows slow relaxation in **2**, but not in **1** or **3** down to 2 K and up to 1 kHz.

1. Introduction

Molecular magnets differ from more conventional elemental, alloyed, and metal–oxide magnets in many ways. Rather than being composed of one or two atom types, molecular magnets have paramagnetic centers intercalated with organic constituents to yield complicated crystal lattices. The high degree of tailorability through synthesis has yielded multitudinous magnetic materials, often exploited towards understanding fundamental physical science concepts and increasingly with the hopes of technological application.[1] One specific application that has been heavily researched is single-molecule magnetism (SMM), in which it is hoped that single molecules may display magnetic hysteresis that would provide extremely high density data storage.[2] Correspondingly, these systems have the potential for molecular level spintronics[3] and usage as qubits in quantum computers.[4]

The state of the art rests on a storied history, but we highlight a few relevant, bellwether discoveries. The seminal compound of the field is $Mn_{12}Ac_{16}$ (ac = acetate), reported in 1991 to have an $S = 10$ molecular ground state,[5] which shows a slow relaxation of magnetization at low temperatures. Along these lines, many different transition metal containing clusters were reported to have similar effects in the following years.[6] However, the energy barrier that locks the angular momentum in a specific orientation is always well below the thermal energy available at room temperature, and generally even cryogenic temperatures cannot lock the magnetization in a fixed state that could be measured at a significantly later time to encode information. Many approaches have been tried to increase this energy barrier, and one notable scheme is the incorporation of lanthanide elements into molecular magnets, as displayed in a 2003 report detailing Dy^{3+} and Tb^{3+} double-decker phthalocyanine molecules.[7] Furthering motivation for this line of work, in 2007 an experiment on Er^{3+}:$CaWO_4$ showed the strikingly long coherence time possible by a rare-earth qubit.[8] Over the last decade, the discipline of rare-earth SMMs has continued to blossom, yielding an increasing number of examples of systems showing slow relaxation of magnetization at cryogenic temperatures.[9]

Among the lanthanide ions, dysprosium has been the most proliferous progenitor of SMMs, presumably benefitting from the large first-order orbital angular momentum component that may be strongly coupled to orient the total angular momentum with the lattice.[10] Already, a number of Dy^{3+}-containing compounds exhibiting different topologies have been described in the literature,[11] and noteworthy structures include monomeric magnetic centers,[12] dimers,[13] linear trinuclear molecules,[14] triangles,[15] defect-dicubane,[16] square-pyramidal,[17] and a wheel.[18] This universality strongly suggests that single-ionic effects are of a high importance. Another interesting twist on Dy^{3+}-based SMMs was recently reported in

[a]*National Institute of Standards and Technology, Gaithersburg, Maryland 20899, USA. E-mail: daniel.pajerowski@nist.gov*
[b]*Key Laboratory of Functional Inorganic Material Chemistry (MOE), P. R. China; School of Chemistry and Materials Science, Heilongjiang University, No. 74, Xuefu Road, Nangang District, Harbin 150080, P. R. China. E-mail: gmli_2000@163.com*
[c]*Department of Chemical Engineering and Materials Science, University of Minnesota, Minneapolis, Minnesota 55455, USA*
[d]*Montgomery Blair High School, Silver Spring, Maryland 20901, USA*
†CCDC 851931 (**1**), 851932 (**2**) and 851933 (**3**). For crystallographic data in CIF or other electronic format see DOI: 10.1039/c4dt01329h

which slow-relaxation could be tuned with (de)hydration.[19] An alternative lanthanide that has shown slow relaxation in many molecular compounds is the trivalent erbium ion.[20] Also possessing large first-order orbital angular momentum and a large total moment with more than a half-full shell of valence electrons, there are many similarities between erbium and dysprosium electronic structures.

In view of the recent reports on the structures and important magnetism of multi-nuclear lanthanide complexes[21] and our long-standing study on the synthesis and properties of multi-nuclear lanthanide complexes,[22] we attempted to synthesize a series of *N*,*N*′-bis(salicylidene)-1,2-(phenylenediamine) polynuclear lanthanide complexes to look for slow magnetic relaxation. However, three new chloride-bridged lanthanide compounds with unique defect-dicubane {Ln4} [Ln = Gd (**1**), Dy (**2**) and Er (**3**)], core were accidentally isolated instead. We report here the synthesis, structure, direct current (DC), and alternating current (AC) magnetization studies of **1–3**. The DC magnetization can be well understood as interacting anisotropic ions, and we observe slow magnetic relaxation in **2** from the AC susceptibility without any bias field.

2. Experimental[23]

2.1. Reagents and general techniques

All chemicals except $LnCl_3{\cdot}6H_2O$ were obtained from commercial sources and used without further purification. $LnCl_3{\cdot}6H_2O$ (Ln = Gd, Dy and Er) was prepared by the reactions of a lanthanide oxide and hydrochloric acid. Elemental analyses were performed on a Perkin-Elmer 2400 analyzer. The DC magnetizations of compounds **1–3** were measured with a Quantum Design MPMS superconducting quantum interference device (SQUID) magnetometer and the AC data were measured with a Quantum Design MPMS-XL SQUID magnetometer; magnetization was measured over the range 2 K to 300 K in constant 0.1 T applied field, isothermal magnetization was measured at 2 K from −7 T to 7 T, and AC susceptibility was measured at 31.6 Hz, 200 Hz, and 997 Hz in an oscillating field of 0.4 mT and zero bias field. Powder samples were mounted in gelatin capsules for SQUID studies. Diamagnetic corrections to DC magnetization were made using Pascal's constants for the constituent molecules, and the sample mounts are at or below the noise of the measurement.

2.2. Synthesis

Compounds **1–3** were prepared by the reactions of a solution of $LnCl_3{\cdot}6H_2O$ (0.1 mmol) in MeOH (5 mL) with a solution of H_2L (0.0632 g, 0.2 mmol) in CH_2Cl_2 (25 mL). The mixed solution was stirred for 4 hours under ambient temperature and subsequently filtered to remove the suspended particles. Block crystals were obtained by slow diffusion of diethylether into the filtrate after approximately one week. Elemental analysis (%) Calc. For **1**, $C_{14}H_{58}Cl_{10}Gd_4O_{16}$ (1466.10): C, 11.47; H, 3.99. Found: C, 11.45; H, 4.03. Elemental analysis (%) Calc. For **2**, $C_{14}H_{58}Cl_{10}Dy_4O_{16}$ (1487.10): C, 11.31; H, 3.93. Found: C, 11.28; H, 3.94. Elemental analysis (%) Calc. For **3**, $C_{14}H_{58}Cl_{10}Er_4O_{16}$ (1506.14): C, 11.16; H, 3.88. Found: C, 11.14; H, 3.92.

2.3. X-ray crystallographic determination

Suitable single crystals of **1**, **2** and **3** were selected for room temperature (20 °C ± 2 °C) X-ray diffraction analysis with a Siemens SMART CCD diffractometer using graphite-monochromated Mo-Kα radiation (λ = 0.71073 Å). These data were processed with the SAINT processing program.[24] Crystal structures were solved by direct methods and refined on F^2 by full-matrix least-squares using the SHELXTL-97 program.[25] Due to the high symmetry, the Cl5 and Cl6 ion positions are disordered and distributed between two crystallographic sites in complexes **1**, **2**, and **3**. All non-hydrogen atoms are anisotropically refined.

3. Results and discussion

3.1. Structural description

X-ray crystallographic analysis reveals that compounds **1–3** are isomorphic, and we discuss the structures in the context of **1**. Beginning with the magnetic cations, four Gd^{3+} ions are bridged by six Cl^- ions to compose a defect-dicubane $\{Gd_4Cl_6\}^{6+}$ core, which is charge-balanced by two hydroxyl radicals and four additional uncoordinated Cl^- ions, as shown in Fig. 1. Methanol groups are also observed, both within the rare-earth cluster and dissociated among the host structure between rare-earth clusters. Within the $\{Gd_4Cl_6\}$ core, any two Gd^{3+} ions ostensibly have two Cl^- ions between them. There are two crystallographically distinct Gd^{3+} ions that are both seven-coordinated in a distorted pentagonal bipyramid geometry. The $Gd(1)^{3+}$ ion is seven-coordinated to three oxygen atoms from three methanol molecules and four Cl^- ions, while the $Gd(2)^{3+}$ ion is seven-coordinated to one OH^- group, three oxygen atoms from methanols, and three Cl^- ions (Fig. 1). The $Gd(1)^{3+}$ and $Gd(2)^{3+}$ ions are bridged by two Cl^- ions. The Gd(1)–Gd(1A) distance is 3.6137(10) Å, while the Gd(1)–Gd(2) and Gd(1)–Gd(2A) distances are 3.9919(11) Å and 3.9991(11) Å, respectively. The Gd(2)–Gd(2A) distance is appreciably longer than other intra-cluster Gd separations at

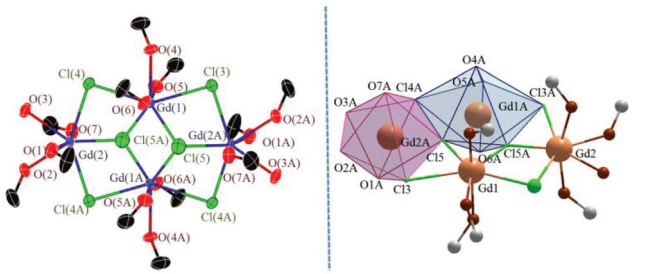

Fig. 1 The cationic core of compound **1**. (left) From crystallography data, displacement ellipsoids are drawn at the 50% probability level (hydrogen atoms are omitted for clarity). (right) To emphasize the coordination sphere, the polyhedral coordination geometry of Gd^{3+} ions in the asymmetric unit of compound **1** is shown.

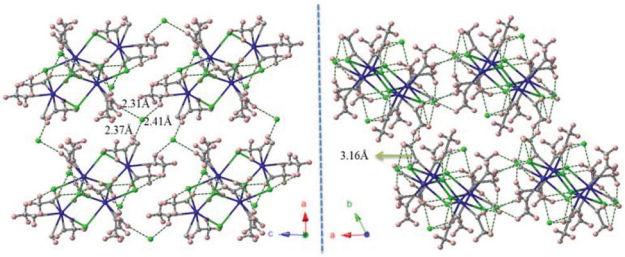

Fig. 2 The packing structural unit of compound **1**. (left) The crystallographic *a* axis is shown. (right) The crystallographic *b* axis is shown. Lanthanides are yellow, oxygens are red, chlorines are green, carbons are black, and hydrogens are white. Dotted lines denote intermolecular H-bonding among Cl^- ions and the oxygen atoms.

7.052(3) Å. For comparison, the inter-cluster Gd separations are 7.294(3) Å, 7.825(3) Å, and 7.223(3) Å, along the *a*, *b*, and *c* axes, respectively. The Gd–O and Gd–Cl distances ranging from 2.358(5) Å to 2.442(4) Å and 2.335(3) Å to 2.8313(16) Å, respectively, are in agreement with reported values.[26] In the packing structure, Fig. 2, there are two types of H-bonding that have been observed among Cl^- ions and the oxygen atoms, from the methanol molecules, in the range of 3.031(6) Å to 3.101(5) Å and among methanol molecules and OH^- groups in the range of 2.712(7) Å to 2.745(7) Å. Noticeably, the synthesizing ligand is not coordinated to the lanthanide ions in complexes **1–3**. However, if synthesis is performed without the ligand, this defect-dicubane core structure is not formed. What we propose is that the defect-dicubane core structure with ligand is formed as an intermediate at the beginning of the reaction. Nevertheless, the ligand dissociation occurs due to the tension of the rigid structure and the weak coordination ability of the tetra-dentate salen-type ligand (*N*,*N*′-bis(salicylidene)-1,2-(phenylene-diamine)) although the dicubane core structure remains. In contrast to the semi-rigid hexa-dentate salen-type ligand, several lanthanide dicubane-like clusters with coordinated ligands have been reported, *e.g.* $[Ln_4(L)_2(HL)_2(\mu_3\text{-}OH)_2Cl_2]\cdot 2Cl$ (Ln = Nd, Yb, Er and Gd; H_2L: *N*,*N*′-bis(salicylidene)cyclohexane-1,2-diamine).[22c] Thus, the ligand plays essential role on the formation of the dicubane like cluster.

3.2. Magnetic properties

For these clusters, the most interesting aspect of the magnetism is the potential for SMM behavior, whereby a thermal barrier (U_{eff}) exists between reversals of the ground state magnetization orientation of a cluster. Towards discernment of the potential for a finite U_{eff}, we begin with analysis of the DC magnetic properties. As the magnetic electrons in these systems are highly localized, the relevant energies for a single ion are intra-atomic Coulomb interactions (H_{C}), spin–orbit coupling ($H_{\mathrm{S-O}}$), crystalline field (H_{CF}), and magnetic fields (H_{mag}, both internal and external). Therefore, in the rare-earth regime of $H_{\mathrm{C}} \approx H_{\mathrm{S-O}} \gg H_{\mathrm{CF}} \approx H_{\mathrm{mag}}$ our analysis begins with the well-known free-ion wavefunctions of $H_{\mathrm{C}} + H_{\mathrm{S-O}}$,[27] and the higher-order interactions are diagonalized from the total-angular momentum basis. We consider electrostatic and electromagnetic contributions due to the lattice as a starting point and, from there, argue for the presence of additional interactions. Explicitly, the crystal field Hamiltonian is written using Stevens operators in the method of operator equivalents,[28]

$$H_{\mathrm{CF}} = \sum_{n=0}^{6}\sum_{m=0}^{n} B_n^m \hat{O}_n^m, \tag{1}$$

$$B_n^m = A_{n,m}\langle r\rangle^n \theta_n \Lambda_n, \tag{2}$$

where the parameters $A_{n,m}$ depend upon the specifics of the crystal, r^n are the expectation values of the free-ion radial wavefunctions, θ_n are the parameters of Elliot and Stevens intrinsic to the method of operator equivalents, Λ_n are empirical parameters that may account for effects like screening and covalence, and the operators $\hat{O}_n^m$ are linear combinations of angular momentum operators up to the order '*m*.' To obtain electrostatic potentials, we performed a linear combination of atomic orbitals density functional theory calculation[29] for each of the individual organic constituent molecules, namely, the methanol group and the hydroxyl radical. Effective point-charges were extracted from the calculated Mulliken populations, and the effective methanol point-charges were scaled down to match the dipole moment of the complete density functional theory charge density map. Chlorine and lanthanide ions were taken to have their formal charges of −1 and +3, respectively. For a given magnetic center, potentials were then calculated for distances up to nominally 26 Å where $A_{n,m}$ values show convergence within less than 1% deviation. The magnetostatic Hamiltonian contains dipolar coupling, Zeeman energy, and a superexchange interaction such that

$$\begin{aligned} H_{\mathrm{mag}} = & -\sum_{j,k}\frac{\mu_0}{4\pi r_{jk}^3}\begin{pmatrix} 3\left(g_{\mathrm{J},j}\mu_{\mathrm{B}}\hat{\mathbf{J}}_j\cdot\mathbf{e}_{jk}\right)\left(g_{\mathrm{J},k}\mu_{\mathrm{B}}\hat{\mathbf{J}}_k\cdot\mathbf{e}_{jk}\right)\cdots \\ \cdots - g_{\mathrm{J},j}g_{\mathrm{J},k}\mu_{\mathrm{B}}{}^2\hat{\mathbf{J}}_j\cdot\hat{\mathbf{J}}_k \end{pmatrix}, \\ & -\sum_i g_{\mathrm{J},i}\mu_{\mathrm{B}}\mu_0\hat{\mathbf{J}}_i\cdot\mathbf{H} + H_{\mathrm{SX}} \end{aligned} \tag{3}$$

where μ_0 is the vacuum permeability ($4\pi \times 10^{-7}$ V s (A m)$^{-1}$), r_{jk} is the distance between two magnetic ions, g_{J} is the Landé factor for total angular momentum, μ_{B} is a Bohr magneton ($9.27400968 \times 10^{-24}$ J T^{-1}), $\hat{\mathbf{J}}$ is an angular momentum operator, $\mathbf{e}$ is the unit vector connecting two magnetic ions, $\mathbf{H}$ is the applied magnetic field, the summations are taken over all magnetic atoms within a cluster, and H_{SX} takes into account spin–spin correlations, though we still work with total angular momentum operators, such that

$$\begin{aligned} H_{\mathrm{SX}} = & J_{1,1\mathrm{A}}\hat{\mathbf{J}}_1\cdot\hat{\mathbf{J}}_{1\mathrm{A}} + J_{1,2}\hat{\mathbf{J}}_1\cdot\hat{\mathbf{J}}_2 + J_{2,1\mathrm{A}}\hat{\mathbf{J}}_2\cdot\hat{\mathbf{J}}_{1\mathrm{A}} + J_{1\mathrm{A},2\mathrm{A}}\hat{\mathbf{J}}_{1\mathrm{A}}\cdot\hat{\mathbf{J}}_{2\mathrm{A}} \\ & + J_{2\mathrm{A},1}\hat{\mathbf{J}}_{2\mathrm{A}}\cdot\hat{\mathbf{J}}_1, \end{aligned} \tag{4}$$

where J is an effective, isotropic superexchange energy and subscripts keep track of interaction pairs on different crystallographic sites. Magnetization is calculated in the usual way with statistical mechanics, and powder averaging is done by

Table 1 Crystal data and structure refinement for compounds **1–3**

	1	**2**	**3**
CCDC no.	851931	851932	851933
Empirical formula	$C_{14}H_{58}Cl_{10}Gd_4O_{16}$	$C_{14}H_{58}Cl_{10}Dy_4O_{16}$	$C_{14}H_{58}Cl_{10}Er_4O_{16}$
Formula weight	1466.10	1487.10	1506.14
Crystal system	Triclinic	Triclinic	Triclinic
Space group	$P\bar{1}$	$P\bar{1}$	$P\bar{1}$
a (Å)	10.357(2)	10.328(2)	10.283(2)
b (Å)	10.675(2)	10.653(2)	10.613(2)
c (Å)	11.716(2)	11.639(2)	11.585(2)
α (°)	87.65(3)	87.55(3)	87.48(3)
β (°)	86.18(3)	86.14(3)	86.09(3)
γ (°)	62.59(3)	62.66(3)	62.75(3)
V (Å^3)	1147.3(4)	1134.8(4)	1121.3(4)
Z	1	1	1
$D_{calc'd}$ (mg cm^{-3})	2.122	2.176	2.231
F (000)	696	704	712
M (Mo Kα) (mm^{-1})	6.336	7.147	8.053
θ Range (°)	3.49–27.48	3.51–27.48	3.53–27.48
Reflection collected	11 327	11 167	11 095
Unique reflections	5193	5148	5086
R_{int}	0.0622	0.0431	0.0342
R_1, wR_2 ($I > 2\sigma(I)$)	0.0333, 0.0813	0.0422, 0.1084	0.0303, 0.0727
R_1, wR_2 (all data)	0.0394, 0.0842	0.0467, 0.1112	0.0348, 0.0751
GOF on F^2	1.048	1.066	1.065
$\Delta\rho$ (e Å^{-3})	1.143, −0.922	3.994, −1.602	2.517, −1.024

calculating 100 different orientations of the magnetic field with respect to the crystal. Field orientations were chosen with a spiral approximation to sphere coverage.[30] Although our crystals are monoclinic, it is useful to have an orthogonal coordinate system for calculations, and one such possible basis that we employ is $y \| b$, $z \| (a \times b)$, and $x \| (y \times z)$. Experimentally, the magnetic signals are expressed per mole of powder using the chemical formulas listed in Table 1.

For **1**, the free-ion ground term of Gd^{3+} is $4f^7$ ($^8S_{7/2}$, $J = 7/2$, $S = 7/2$, $L = 0$, $g_J = 2$), with the next excited state some 30 000 cm^{-1} (4 eV) higher in energy.[31] A crystalline electric field does not split this state, but magnetic susceptibility, Fig. 3, and high-field magnetization, Fig. 4, show a slight departure from the free-ion term for four gadolinium ions ($\mu_{eff}^2[Gd_{free}^{3+}] = 4g_J^2\mu_B^2J(J+1) = 252.00\mu_B^2$, $M_{sat}[Gd_{free}^{3+}] = 4g_J\mu_BJ = 28.00\mu_B$), mainly at low temperatures. Therefore, a small unaccounted for interaction such as inter-ionic antiferromagnetic superexchange or a crystalline-field-like single-ion energy (due to lattice perturbations distorting the spin–orbit wavefunction) may be present. While powder-averaged measurements cannot unambiguously assign such an energy, they can estimate upper-limits to its contribution. A fit including H_{SX}, Fig. 3 and 4, shows how $J_{1,2} = J_{2,1A} = J_{1A,2A} = J_{2A,1} = 0.06$ cm^{-1} (0.007 meV) (or adding B_2^0 the same order of magnitude) improves the agreement with experiment, although near perfect agreement is possible but highly equivocal when phenomenologically co-fitting H_{SX} and the B_n^m's of H_{CF} to powder data (Table 2).

For **2**, the single-ion behavior is immediately more complicated, as a crystalline electric field does preferentially align the oblate spheroid, ground-state Dy^{3+} charge density. A free Dy^{3+} ion is $4f^9$ ($^6H_{15/2}$, $J = 15/2$, $S = 5/2$, $L = 5$, $g_J = 4/3$), with a spin–orbit coupling parameter of 1820 cm^{-1} (226 meV),[31] but this $^6H_{15/2}$ term is split into 8 doublets by the low symmetry H_{CF} of **2**, Table 3. The resulting ground-state anisotropy axes of H_{CF} are visualized in Fig. 5. Indeed, the ground state anisotropy axes as determined by the electrostatic crystalline field have been shown to be quite accurate for dysprosium cluster complexes.[32] Upon comparison with the experimental data, a curious feature not captured by non-interacting anisotropic ions is the broad hump in the temperature dependence of the

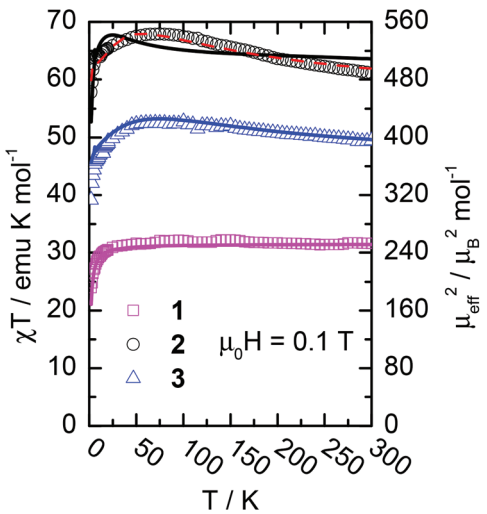

Fig. 3 Temperature dependence of the χT product. The symbols are experimental data and solid lines are fits of superexchange intra-cluster interactions as described in the text. The red dashed line shows how additional fitting screening parameters of the crystal field can improve the quality of fit for **2**.

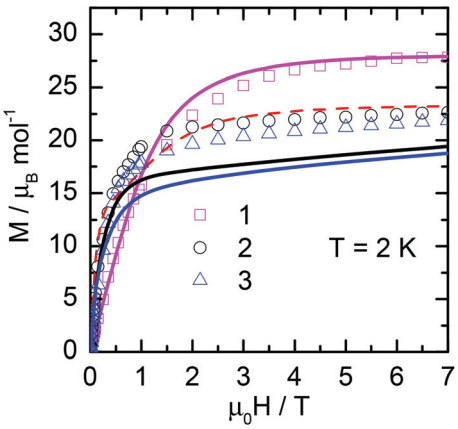

Fig. 4 Field dependence of the magnetization. The symbols are experimental data and solid lines are fits of superexchange intra-cluster interactions as described in the text. The point-charge derived single-ion parameters for the clusters systematically underrepresent the experimental values of high-field magnetization, and possible reasons for this incongruity are described in the text. As one possible candidate for improving agreement between model and experiment, the red dashed line shows how additionally fitting screening parameters of the crystal field can improve the quality of fit for **2**.

Table 2 Selected bond lengths (Å) and angles (°) for compounds **1–3**

	1	**2**	**3**
Ln(1)–O(6)	2.376(5)	2.344(5)	2.319(5)
Ln(1)–O(5)	2.381(5)	2.363(6)	2.328(5)
Ln(1)–Cl(5)	2.407(4)	2.388(5)	2.377(4)
Ln(1)–O(4)	2.442(4)	2.419(5)	2.398(5)
Ln(1)–Cl(3)	2.8305(17)	2.812(2)	2.7932(18)
Ln(1)–Cl(4)	2.8313(16)	2.805(19)	2.7857(17)
Ln(1)–Ln(2)	3.6137(10)	3.9551(11)	3.9198(11)
Ln(2)–O(1)	2.358(6)	2.335(6)	2.310(5)
Ln(2)–O(7)	2.358(5)	2.329(6)	2.300(5)
Ln(2)–O(3)	2.408(4)	2.381(6)	2.357(5)
Ln(2)–O(2)	2.437(5)	2.420(6)	2.388(5)
Ln(2)–Cl(4)	2.7760(16)	2.7654(19)	2.7390(17)
Cl(3)–Ln(1)–Cl(5)	71.87(10)	71.83(12)	71.85(11)
Cl(5)–Ln(1)–Cl(5A)	81.727(15)	81.210(15)	81.723(15)
Cl(5A)–Ln(1)–Cl(4)	70.758(10)	71.069(13)	71.205(12)
Cl(4)–Ln(2)–Cl(5A)	72.533(9)	72.747(12)	72.641(12)
Cl(5A)–Ln(2)–Cl(3A)	72.118(15)	72.366(12)	72.680(11)
Ln(2)–Cl(4)–Ln(1)	90.78(4)	90.47(5)	90.39(5)
Ln(2)–Cl(5)–Ln(1)	114.75(18)	115.16(18)	114.36(16)
Ln(2)–Cl(5)–Ln(1A)	115.307(16)	116.238(20)	115.052(18)
Ln(2)–Cl(5)–Ln(1)	115.687(18)	115.546(19)	114.889(19)
Ln(2)–Cl(3A)–Ln(1A)	90.901(6)	90.439(7)	90.314(6)

Table 3 Energy eigenvalues of the electrostatic H_{CF} in meV for the different crystallographic sites of **2** and **3**

Dy(1,1A)	Dy(2,2A)	Er(1,1A)	Er(2,2A)
0	0	0	0
27	19	8	8
50	35	15	13
68	49	21	17
81	59	27	21
96	69	33	26
115	84	41	31
138	102	50	38

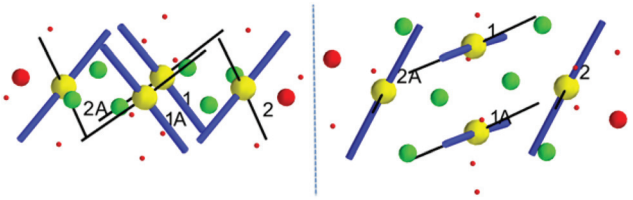

Fig. 5 A view nearly parallel to the {Ln_4} plane (top) and perpendicular to the {Ln_4} plane (bottom) illustrate the ground-state anisotropy axes determined by the local electric field for **2** (thin black line) and **3** (thick blue line). The coordination spheres of the magnetic ions are shown, with spherical volumes scaled to the ionic charge. Lanthanides are yellow, oxygens are red, and chlorines are green.

effective moment, Fig. 3, that coincides with an overall increase in susceptibility at high temperatures compared to the value for four free Dy^{3+} ions ($\mu_{eff}^2[Dy_{free}^{3+}] = 4g_J^2\mu_B^2J(J+1) = 453.33\mu_B^2$), suggesting the presence of ferromagnetic interactions in the system. Indeed, such an increase followed by a decrease in the effective moment while cooling is consistent with ferromagnetically coupled anisotropic ions. Furthermore, this feature in susceptibility is also seen in other defect dicubane clusters.[16f] It is worth noting that the confluence of dipolar coupling with high-anisotropy does already give a ferromagnetic-like correlation for this cluster, but the aspect is far too small to create a maximum like that observed in the data. The saturation magnetization is drastically reduced from that for four free ions ($M_{sat}[Dy_{free}^{3+}] = 4g_J\mu_BJ = 40.00\mu_B$), Fig. 4, which is due to the presence of a large anisotropy, although the experimental observation is still larger than a simple powder averaged $J = 15/2$ doublet in the large uniaxial anisotropy limit ($\langle\cos^2\theta\rangle 40.00\mu_B = 20.00\mu_B$). A fair reproduction of the experimental results is possible by including intra-cluster interactions such that $J_{1,2} = J_{2,1A} = J_{1A,2A} = J_{2A,1} = -0.8$ cm^{-1} (−0.1 meV) and $J_{1,1A} = 0.4$ cm^{-1} (0.04 meV), Fig. 3 and 4. This fit to the temperature dependent effective moment shows the qualitative increase in susceptibility at high temperatures, along with a finite positive slope on cooling that eventually goes through a maximum and decreases.

For **3**, Er^{3+} has a ground-state charge density that is more like a prolate spheroid, which also has preferential alignment in a crystal field. The Er^{3+} ion is $4f^{11}$ ($^4I_{15/2}$, $J = 15/2$, $S = 3/2$, $L = 6$, $g_J = 6/5$), with the next excited state 6 500 cm^{-1} (810 meV) higher in energy and a spin orbit coupling parameter of 2 360 cm^{-1} (293 meV), but this $^4I_{15/2}$ term is split into 8 doublets by the local electric field of **3**, Table 3. The resulting ground-state anisotropy axes of H_{CF} are visualized in Fig. 5. Not surprisingly, **3** also shows a large departure in the magnetic properties expected for four non-interacting erbium ions in the magnetic cluster ($\mu_{eff}^2[Er_{free}^{3+}] = 4g_J^2\mu_B^2J(J+1) = 367.20\mu_B^2$, $M_{sat}[Er_{free}^{3+}] = 4g_J\mu_BJ = 36.00\mu_B$), having an increased high temperature susceptibility with a strong temperature dependence, Fig. 3, as well as a greatly diminished saturation magnetization compared to free Er^{3+}, Fig. 4. Reminiscent of **2**, the saturation magnetization is still larger than simple powder averaged $J = 15/2$ doublets in the large uni-

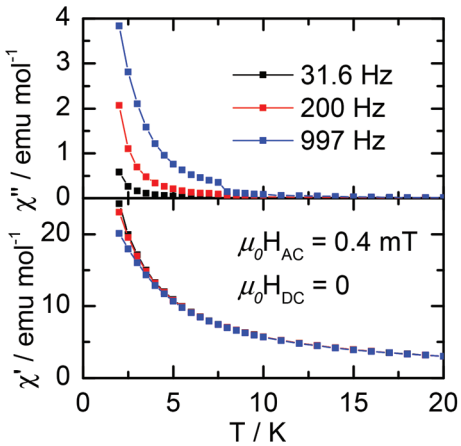

Fig. 6 Temperature dependence of the AC susceptibility at different frequencies for the dysprosium cluster (**2**).

axial anisotropy limit ($\langle\cos^2\theta\rangle 36.00\mu_B = 18.00\mu_B$). Fitting only isotropic superexchange parameters, $J_{1,2} = J_{2,1A} = J_{1A,2A} = J_{2A,1} = -0.5$ cm^{-1} (−0.06 meV), can capture many features of the data.

To check for slow relaxation, frequency dependent AC susceptibility measurements were performed on samples **1**, **2**, and **3** without any bias field to avoid confusion with simple paramagnetic precession. Of the three, only the dysprosium sample (**2**) showed an effect under our experimental conditions, Fig. 6. While clear phase shifting occurs, we do not observe a peak and therefore do not try to extract an activation energy. In the context of our series, it is logical that **2** is the only sample to show frequency dependence, as it has the largest anisotropy barrier coming from the crystal field.

We now suggest possibilities for the discrepancies between model calculations and the experimental data. The largest quantitative incongruity is in the isothermal magnetizations of **2** and **3**, although improvement in the fit of the susceptibility of **2** would also be desirable. We discuss potential corrections in the context of **2**. To begin, in some sense it is serendipitous that a simple point-charge calculation does such a good job at estimating H_{CF}. By introducing more parameters into the fit, namely $\Lambda_2 = 0.2$, $\Lambda_4 = 0.8$, and $\Lambda_6 = 8$ in eqn (2), the residuals may be greatly reduced for both susceptibility and isothermal magnetization, Fig. 3 and 4. The ability to preferentially screen out lower order terms in H_{CF} is not unprecedented and is ascribed to deformation of the outer 5s and 5p electrons in a response to the crystalline field.[33] A specific study on modifications to point charge models related to lanthanide SMMs also showed that screened charges better reproduced their experimental data.[34] However, the way the saturation moment is increased is by de-stabilizing the doublet with the most J = 15/2 character on the 2 and 2A dysprosium site, and a level crossing can be seen around 1 T as inflection in the magnetization, which is hard to physically motivate. Similar model curve-shapes can be generated by allowing for a more complicated spin correlation than in eqn (4), and an anisotropic superexchange can simultaneously fit the temperature dependent moment and increase the powder saturation magnetization. Incidentally, a recent report invoked anisotropic exchange to explain behavior in a 3d–5d transition metal SMM.[35] Without additional evidence, such as an angular dependent single crystal spectroscopy, the origin of the interaction that increases the magnetizability at high fields for the components transverse to the easy axis remains nebulous. Circumstantially, the presence of slow relaxation due to stabilization of a large moment Kramer's doublet ground state concomitant with anomalously high saturation moments suggests a missing cluster interaction energy rather than a single-ion destabilization of the ground-state.[11–18] To tackle this problem from a computational standpoint, it would also be interesting to see if a high magnetic field, density functional theory calculation of a dysprosium cluster could give rise to such effects.

4. Conclusions

Three new compounds, $[Gd_4Cl_6(CH_3OH)_{12}(OH)_2]\cdot 4Cl\cdot 2CH_3OH$ [Ln = Gd (**1**), Dy (**2**) and Er (**3**)], were accidentally isolated by the interruption of the salen type ligand of *N*,*N*′-bis(salicylidene)-1,2-(phenylene-diamine). This interruption seems to dominate the formation of the compounds featuring the chloride-bridged defect-dicubane $\{Ln_4\}$ core. Magnetic properties are mainly due to single-ion effects, but interactions within clusters must be included to reproduce the experimental data, showing dominant antiferromagnetic correlations in **1**, and ferromagnetic correlations in **2** and **3**. Finally, for the Dy^{3+} sample, we observe slow magnetic relaxation that is suggestive of single-molecule magnet properties in this material.

Acknowledgements

This work is financially supported by the National Natural Science Foundation of China (no. 51272069). DMP and JH gratefully acknowledge the Summer High-school Internship Program (SHIP) at the National Institute of Standards and Technology (NIST) Center for Neutron Research, the financial support provided by NIST and the Center for High Resolution Neutron Scattering (CHRNS), and the usage of facilities supported, in part, by the National Science Foundation under Agreement no. DMR-0944772.

Notes and references

1 J. S. Miller and A. J. Epstein, Molecule-Based Magnets—An Overview, *MRS Bull.*, 2000, **25**, 21.
2 (*a*) H. J. Eppley, H.-L. Tsai, N. devries, K. Folting, G. Christou and D. N. Hendrickson, *J. Am. Chem. Soc.*, 1995, **117**, 301; (*b*) J. D. Rinehart, M. Fang, W. J. Evansand and J. R. Long, *Nat. Chem.*, 2011, **3**, 538; (*c*) L. R. Yang, S. Song, H. M. Zhang, W. Zhang, Z. W. Bu and T. G. Ren, *Synth. Met.*, 2011, **161**, 2230.
3 (*a*) L. Bogani and W. Wernsdorfer, *Nat. Mater.*, 2008, **7**, 179; (*b*) M. Mannini, F. Pineider, C. Danieli, F. Totti, L. Sorace,

P. Sainctavit, M.-A. Arrio, E. Otero, L. Joly, J. C. Cezar, A. Corniaand and R. Sessoli, *Nature*, 2010, **468**, 417.

4 (*a*) G. A. Timco, S. Carretta, F. Troiani, F. Tuna, R. J. Pritchard, C. A. Muryn, E. J. L. Mclnnes, A. Ghirri, A. Candini, P. Santini, G. Amoretti, M. Affronte and R. E. P. Winpenny, *Nat. Nanotechnol.*, 2009, **4**, 173; (*b*) R. Sessoli and A. K. Powell, *Coord. Chem. Rev.*, 2009, **253**, 2328.

5 A. Caneschi, D. Gatteschi, R. Sessoli, A. L. Barra, L. C. Brunel and M. Guillot, *J. Am. Chem. Soc.*, 1991, **113**, 5873–5874.

6 D. Gatteschi, R. Sessoli and J. Villain, *Molecular Nanomagnets*, Oxford University Press, Oxford, U.K., 2006.

7 N. Ishikawa, M. Sugita, T. Ishikawa, S. Koshihara and Y. Kaizu, *J. Am. Chem. Soc.*, 2003, **125**, 8694.

8 S. Bertaina, S. Gambarelli, A. Tkachuk, I. N. Kurkin, B. Malkin, A. Stepanov and B. Barbara, *Nat. Nanotechnol.*, 2007, **2**, 39.

9 (*a*) J. Luzon, K. Bernot, I. J. Hewitt, C. E. Anson, A. K. Powell and R. Sessoli, *Phys. Rev. Lett.*, 2008, **100**, 247205; (*b*) L. Chibotaru, L. Ungur and A. Soncini, *Angew. Chem., Int. Ed.*, 2008, **47**, 4126; (*c*) C. M. Zaleski, E. C. Depperman, J. W. Kampf, M. L. Kirk and V. L. Pecoraro, *Angew. Chem., Int. Ed.*, 2004, **43**, 3912; (*d*) C. Aronica, G. Pilet, G. Chastanet, W. Wernsdorfer, J.-F. Jacquot and D. Luneau, *Angew. Chem., Int. Ed.*, 2006, **45**, 4659; (*e*) J.-P. Costes, S. Shova and W. Wernsdorfer, *Dalton Trans.*, 2008, 1843; (*f*) C. E. Burrow, T. J. Burchell, P.-H. Lin, F. Habib, W. Wernsdorfer, R. Clerac and M. Murugesu, *Inorg. Chem.*, 2009, **48**, 8051; (*g*) Y.-Z. Zheng, Y. Lan, C. E. Anson and A. K. Powell, *Inorg. Chem.*, 2009, **47**, 10813; (*h*) G.-F. Xu, Q.-L. Wang, P. Gamez, Y. Ma, R. Clerac, J. Tang, S.-P. Yan, P. Cheng and D.-Z. Liao, *Chem. Commun.*, 2010, **46**, 1506; (*i*) S. K. Langley, B. Moubaraki, C. M. Forsyth, I. A. Gass and K. S. Murray, *Dalton Trans.*, 2010, **39**, 1705.

10 Y.-N. Guo, G.-F. Xu, Y. Guo and J. Tang, *Dalton Trans.*, 2011, **40**, 9953.

11 (*a*) B. Hussain, D. Savard, T. J. Burchell, W. Wernsdorfer and M. Murugesu, *Chem. Commun.*, 2009, 1100; (*b*) R. Liu, L. Li, X. Wang, P. Yang, C. Wang, D. Liao and J.-P. Sutter, *Chem. Commun.*, 2010, **46**, 2566; (*c*) Y. Wang, X. L. Li, T. W. Wang, Y. Song and X. Z. You, *Inorg. Chem.*, 2010, **49**, 969; (*d*) Y.-N. Guo, G.-F. Xu, P. Gamez, L. Zhao, S.-Y. Lin, R. Deng, J. Tang and H.-J. Zhang, *J. Am. Chem. Soc.*, 2010, **132**, 8538.

12 (*a*) V. E. Campbell, H. Bolvin, E. Rivière, R. Guillot, W. Wernsdorfer and T. Mallah, *Inorg. Chem.*, 2014, **53**, 2598; (*b*) V. E. Campbell, R. Guillot, E. Riviere, P.-T. Brun, W. Wernsdorfer and T. Mallah, *Inorg. Chem.*, 2013, **52**, 5194; (*c*) S.-D. Jiang, B.-W. Wang, G. Su, Z.-M. Wang and S. Gao, *Angew. Chem., Int. Ed.*, 2010, **49**, 7448; (*d*) C.-M. Liu, D.-Q. Zhang and D.-B. Zhu, *Inorg. Chem.*, 2013, **52**, 8933; (*e*) Y. Bi, Y.-N. Guo, L. Zhao, Y. Guo, S.-Y. Lin, S.-D. Jiang, J. Tang, B.-W. Wang and S. Gao, *Chem. – Eur. J.*, 2011, **17**, 12476; (*f*) J. Long, R. Vallat, R. A. S. Ferreira, L. D. Carlos, F. A. Almeida Paz, Y. Guari and J. Larionova, *Chem. Commun.*, 2012, **48**, 9974; (*g*) G.-J. Chen, C.-Y. Gao, J.-L. Tian, J.-K. Tang, W. Gu, X. Liu, S.-P. Yan, D.-Z. Liao and P. Cheng, *Dalton Trans.*, 2011, **40**, 5579.

13 (*a*) P. H. Lin, T. J. Burchell, R. Clerac and M. Murugesu, *Angew. Chem., Int. Ed.*, 2008, **47**, 8848; (*b*) R. A. Layfield, J. J. W. McDouall, S. A. Sulway, F. Tuna, D. Collison and R. E. P. Winpenny, *Chem. – Eur. J.*, 2010, **16**, 4442.

14 I. J. Hewitt, Y. H. Lan, C. E. Anson, J. Luzon, R. Sessoli and A. K. Powell, *Chem. Commun.*, 2009, 6765.

15 J. Tang, I. Hewitt, N. T. Madhu, G. Chastanet, W. Wernsdorfer, C. E. Anson, C. Benelli, R. Sessoli and A. K. Powell, *Angew. Chem., Int. Ed.*, 2006, **45**, 1729.

16 (*a*) Y. Z. Zheng, Y. H. Lan, C. E. Anson and A. K. Powell, *Inorg. Chem.*, 2008, **47**, 10813; (*b*) J.-B. Peng, Y.-P. Ren, X.-J. Kong, L.-S. Long, R.-B. Huang and L.-S. Zheng, *CrystEngComm*, 2011, **13**, 2084; (*c*) S. Xue, L. Zhao, Y. Guo, R. Deng, Y. Guo and J. Tang, *Dalton Trans.*, 2011, **40**, 8347; (*d*) Y. Zheng, Y. Lan, C. E. Anson and A. K. Powell, *Inorg. Chem.*, 2008, **47**, 10813; (*e*) P.-H. Guo, J.-L. Liu, Z.-M. Zhang, L. Ungur, L. U. Chibotaru, J.-D. Leng, F.-S. Guo and M.-L. Tong, *Inorg. Chem.*, 2012, **51**, 1233; (*f*) P.-H. Lin, T. J. Burchell, L. Ungur, L. F. Chibotaru, W. Wernsdorfer and M. Murugesu, *Angew. Chem., Int. Ed.*, 2009, **48**, 9489.

17 M. T. Gamer, Y. H. Lan, P. W. Roesky, A. K. Powell and R. Clerac, *Inorg. Chem.*, 2008, **47**, 6581.

18 L. G. Westin, M. Kritikos and A. Caneschi, *Chem. Commun.*, 2003, 1012.

19 M. Ren, D. Pinkowicz, M. Yoon, K. Kim, L.-M. Zheng, B. K. Breedlove and M. Yamashita, *Inorg. Chem.*, 2013, **52**, 8342.

20 R. A. Layfield, *Organometallics*, 2014, **33**, 1084.

21 (*a*) C.-S. Liu, M. Du, E. C. Sanudo, J. Echeverria, M. Hu, Q. Zhang, L.-M. Zhou and S.-M. Fang, *Dalton Trans.*, 2011, **40**, 9366; (*b*) J. Long, F. Habib, P. H. Lin, I. Korobkov, G. Enright, L. Ungur, W. Wernsdorfer, L. F. Chibotaru and M. Murugesu, *J. Am. Chem. Soc.*, 2011, **133**, 5319; (*c*) R. J. Blagg, C. A. Muryn, E. J. L. McInnes, F. Tuna and R. E. P. Winpenny, *Angew. Chem., Int. Ed.*, 2011, **50**, 6530; (*d*) F. Habib, P. H. Lin, J. Long, I. Korobkov, W. Wernsdorfer and M. Murugesu, *J. Am. Chem. Soc.*, 2011, **133**, 8830.

22 (*a*) P. F. Yan, P. H. Lin, F. Habib, T. Aharen, M. Murugesu, Z. P. Deng, G. M. Li and W. B. Sun, *Inorg. Chem.*, 2011, **50**, 7059; (*b*) P. H. Lin, W. B. Sun, M. F. Yu, G. M. Li, P. F. Yan and M. Murugesu, *Chem. Commun.*, 2011, **47**, 10993; (*c*) P. Chen, H. Chen, P. F. Yan, Y. Wang and G. M. Li, *CrystEngComm*, 2011, **13**, 6237; (*d*) P. F. Yan, S. Chen, P. Chen, J. W. Zhang and G. M. Li, *CrystEngComm*, 2010, **13**, 36.

23 Certain commercial equipment, instruments, or materials are identified in this paper to foster understanding. Such identification does not imply recommendation or endorsement by the National Institute of Standards and Technology, nor does it imply that the materials or equipment identified are necessarily the best available for the purpose.

24 *SMART and SAINT software package*, Siemens Analytical X-ray Instruments, Madison, WI, 1996.
25 G. M. Sheldrick, *SHELXTL Program, version 5.1*, Siemens Industrial Automation, Madison, WI, 1997.
26 M. D. Rudd, N. W. Alcock and G. R. Willey, *Inorg. Chim. Acta*, 2003, **353**, 276.
27 A. Abragam and B. Bleaney, *Electron Paramagnetic resonance of Transition Ions*, Clarendon Press, Oxford, UK, 1970.
28 K. W. H. Stevens, *Proc. Phys. Soc. A*, 1952, **65**, 209.
29 (*a*) J. J. Mortensen, L. B. Hansen and K. W. Jacobsen, *Phys. Rev. B: Condens. Matter*, 2005, **71**, 035109; (*b*) J. Enkovaara, C. Rostgaard, J. J. Mortensen, J. Chen, M. Dułak, L. Ferrighi, J. Gavnholt, C. Glinsvad, V. Haikola, H. A. Hansen, H. H. Kristoffersen, M. Kuisma, A. H. Larsen, L. Lehtovaara, M. Ljungberg, O. Lopez-Acevedo, P. G. Moses, J. Ojanen, T. Olsen, V. Petzold, N. A. Romero, J. Stausholm-Møller, M. Strange, G. A. Tritsaris, M. Vanin, M. Walter, B. Hammer, H. Häkkinen, G. K. H. Madsen, R. M. Nieminen, J. K. Nørskov, M. Puska, T. T. Rantala, J. Schiøtz, K. S. Thygesen and K. W. Jacobsen, *J. Phys.: Condens. Matter*, 2010, **22**, 253202.
30 E. B. Saff and A. B. J. Kuijlaars, *Math. Intell.*, 1997, **19**, 5.
31 R. L. Carlin, *Magnetochemistry*, Springer-Verlag, Berlin, 1986.
32 N. F. Chilton, D. Collison, E. J. L. McInnes, R. E. P. Winpenny and A. Soncini, *Nat. Commun.*, 2013, **4**, 2551.
33 R. J. Elliott, *Magnetic Properties of Rare Earth Metals*, Plenum Press, London and New York, 1972.
34 J. J. Baldovi, J. J. Borras-Almenar, J. M. Clemente-Juan, E. Coronado and A. Gaita-Arino, *Dalton Trans.*, 2012, **41**, 13705.
35 V. Hoeke, A. Stammler, H. Bögge, J. Schnack and T. Glaser, *Inorg. Chem.*, 2013, **53**, 257.

